MODELING OF TRANSCUTANEOUS ENERGY TRANSFER SYSTEM FOR AN IMPLANTABLE GASTROINTESTINAL STIMULATION DEVICE

Joanna Liu C. Wu, Martin P. Mintchev

Abstract: *This study models a transcutaneous energy transmission system which can supply DC power to an implanted device without an external battery. The goals of the study are to: (1) develop a model to describe the transcutaneous energy transmission system; and (2) use the developed model to design a transcutaneous energy transmission system for an implantable gastrointestinal neurostimulator. The complete trancutaneous energy system includes a power amplifier, a highly inductive coupling structure, and an ac-to-dc rectifying circuit in the receiver. Power amplification is based on the single-ended class E amplifier concept. The power amplification stage is self-oscillating, and the oscillation frequency is influenced by the coupling of the coils. The highly inductive coupling structure employs the stage tuning concept. Design methods and detailed analysis are provided. The proposed model is verified through the implementation of the design.*

Keywords: *computer modeling, neurostimulation, gastrointestinal disorders*

1. Introduction

1.1 Brief Introduction to the Gastrointestinal System

The gastrointestinal (GI) tract is essentially a long tube stretching from the mouth to the anus as shown in Figure . It includes the esophagus, the stomach, the duodenum, the small intestine, the colon, and the rectum. The functions of GI organs include digestion, absorption, secretion and motility. The GI system is capable of digesting orally accepted material and extracting any useful components from it, then expelling the waste products at the bottom end.

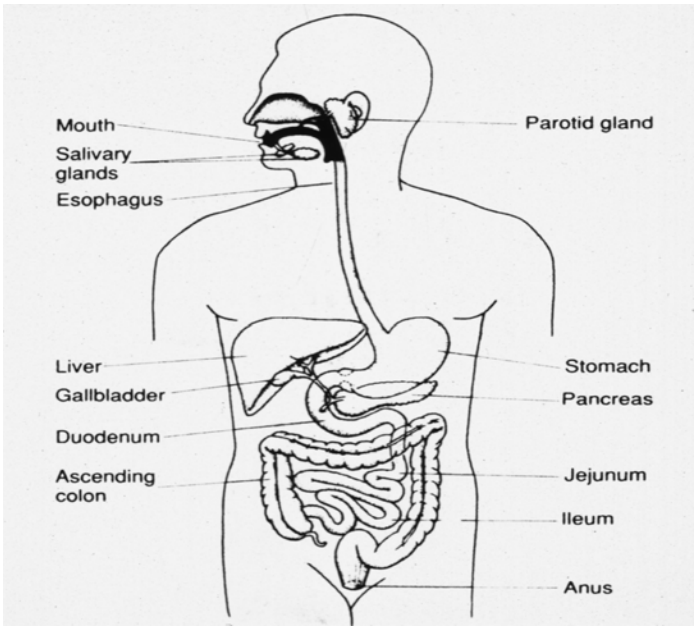

Figure 1: The gastrointestinal tract

1.2 Gastrointestinal Motility

Gastrointestinal motility is defined by the movements of the organs in the digestive system, related to the transit of content in them. For example, on the basis of its motility patterns, the stomach can be divided into two regions. The upper stomach is composed of the fundus and upper corpus. It shows sustained tonic contractions that create basal pressure within the stomach. The lower stomach is composed of the lower corpus and the antrum. It develops strong peristaltic waves of powerful distally propagating contractions that increase in amplitude as they migrate towards the pylorus. Contractions in the distal two-thirds of the stomach occur as a result of the rhythmic depolarization of the gastric smooth muscle cells in annular bands, originating in a region of the proximal corpus usually defined as the gastric pacemaker. Control of gastric contractile activity is mediated through the interaction between both sympathetic and parasympathetic nervous system and the intrinsic electrical activity of the gastric smooth muscle [1]. These gastric slow waves propagate caudally by entraining depolarization in adjacent distal areas of less frequent intrinsic activity. Stronger electrical signals may be superimposed on these slow waves, which are known as spike activity, and have been associated with gastric contractility.

1.3 Gastrointestinal Motility Disorders

Digestive diseases and disorders related to abnormal GI motility patterns occur primarily in the esophagus, the stomach and the colon. The symptoms related to such motility problems may range from gastroesophageal reflux to gastroparesis to constipation. GI disorders are the most common gastrointestinal problems seen by physicians in primary care, and affect millions of people of different ages, including men, women, and children.

Except for the gastroesophageal reflux, which will not be in the focus of the present study, the predominant motility disorders are gastroparesis and constipation, which are explained below in more details.

Gastroparesis is a disease in which the stomach takes too long to empty its contents. It is suggested to be a disorder of the nerves and the smooth muscles of the stomach. The most common symptoms include nausea, vomiting, bloating, feeling full after small meals, and regurgitation. The reasons that cause such a disorder are not fully understood, but diabetic gastroparesis has been clearly identified, and viral causes have been suggested. About 10-20% of gastroparetic cases are of unknown origin and etiology, and are usually labelled as idiopathic gastroparesis. The most common treatment of gastroparesis includes diet changes, medications, and in the most severe cases, parenteral nutrition and partial or total gastrectomy.

Constipation typically refers to dry, difficult, and painful bowel movements related to abnormally delayed colonic transit. The symptoms of constipation include feeling bloated, uncomfortable, and sluggish. Constipation is one of the most common GI complaints in the United States. The data from the 1996 National Health Interview Survey show that about 3 million people in the United States have frequent constipation. Constipation occurs when the colon absorbs too much water or if the colon muscle contractions are slow or sluggish. The main reasons that cause constipation include lack of fiber and liquid intake, lack of exercise, medications, ignoring the urge of bowel movement, problems with the colon and the rectum, etc. Because of the large population suffering from constipation, alternative treatments of this disorder are being investigated [26, 27, 28]. However, in severe cases of idiopathic constipation, partial or total colectomies remain the only presently feasible treatment providing long-term improvements of symptoms.

In the recent years, more and more scientific groups are interested in applying functional electrical stimulation to restore impaired motility in the gastrointestinal tract. There are four distinct methods for GI electrical stimulation. The first method is to entrain slow wave activity in both animals [4] and humans [3] by "pacing" the organ at a frequency slightly higher than the intrinsic slow wave frequency, and approach similar to cardiac pacing. The second method applies current stimulation at 4-40 times the intrinsic slow wave frequency and has been reported to have some antiemetic effect. The most recent stimulation technique is known as neural gastrointestinal

electrical stimulation (NGES) [12, 13]. This approach involves voltage stimulation at 50 Hz delivered through matched pairs of electrodes implanted in the smooth muscle of the stomach wall. The effect of this approach has been shown by accelerated microprocessor-controlled gastric emptying of both solids [10] and liquids [11] in the stomach, as well as by increased colonic transit in both acute and chronic canine models.

The success in the implementation of an NGES system is intimately and directly related to the development of a fully implantable but externally controllable multichannel device. Powering such implanted device becomes a principle challenge. There are four widely accepted techniques for powering an implanted device: (1) Conventional wire cord (focusing on the biocompatibility of the shielding materials), (2) stand-alone implantable battery, (3) radio frequency (RF, transcutaneous inductive) link technologies, and (4) a combination of (2) and (3) using implantable stand-alone rechargeable batteries.

1.4 Aim of the Present Study

The purpose of this feasibility study is to design a transcutaneous power transfer system for a neurostimulator design aiming at restoring impaired gastrointestinal motility. The first mention of powering an implanted device through a transcutaneous inductive coupling link was in 1934 [5]. The practical attempts appeared in the late 1970s [13]. There are two distinct paradigms for designing such a system. One paradigm is known as a loosely coupled link [14] which has a low degree of coupling between the transmitting and the receiving coils, while the other one is highly coupled inductive link, which has a relatively high degree of coupling between the coils. The highly coupled inductive link assumes transmitting and receiving coils of approximately the same size [15] and is the design aim of this project.

2. Methods

2.1 Methods of Power Supply of Implanted Devices

In general, there are four approaches to supply the power to an implanted device: (1) conventional wire cord; (2) battery technologies; (3) RF technologies; and (4) a combination of (2) and (3) using rechargeable batteries. The major advantage of the wire cord approach is technical simplicity. Similar to regular devices, this approach employs power cords and data lines that supply all necessary electrical energy and command signals to the implanted device. Problems of infection, maintenance, and cosmetics hinder the applicability of wired power and data transfer, and therefore, battery-based technologies have been preferred.

Recently developed high energy density batteries increase the life-span of implantable functional devices, making battery-based implants preferable from commercial point of view. However, unlike the technologies of the wired or RF links, which supply both power, and data transmission, the single function of supplying power limits the applicability of battery technologies in implantable devices, since the addition of a separate power-consuming RF link providing device programmability would be necessary. Furthermore, batteries cannot be replaced once they have been implanted, and the patients need to undergo another surgery to replace the batteries. Thus, an implant lasting more than 3 years on a single battery could be reasonably acceptable, but designs with a lower lifespan would be difficult to justify.

The RF approach is believed to be the most promising technique for implantable devices. Its advantages include continuous availability of high levels of power to an implanted device, and the ability to control it with the external device using the same RF link. In addition, the lifetime and shelf life of the implanted devices are not restricted by the life of the battery [16]. The major disadvantage of this approach is the inconvenience for the patient having to permanently wear and external setup providing the transcutaneous link. A combination of having the RF link to recharge an implanted battery converts this permanent inconvenience into an intermittent nuisance. This

approach is typically utilized in cases where the implanted device requires power for a longer period of time than the time that is practical to wear an external transmitter.

2.2 An Overview of Highly Coupling Inductive Link

It has been discussed already that in order to avoid the possibility of infection from piercing the skin and the undesirable replacement of implantable power sources, transcutaneous power transfer is a preferred modality for implantable devices which cannot operate with implantable batteries for more than 3-4 years. This report is concerned with the investigation of the feasibility of utilizing a transcutaneous inductive link for an implanted gastrointestinal stimulation system.

The development of the transcutaneous power technology has been ongoing for several decades. The first attempts to use RF telemetry for providing power to an implanted device took place in 1934 [5]. In late 1970s and early 1980s, practical implantable systems for functional electrical stimulation (FES) applications first appeared [13, 14]. The inductive link employed was called highly coupled stagger-tuned inductive link [15]. The link is a radio-frequency coil system consisting of two same-sized pancake-shaped coils, oriented face-to-face. The primary coil is outside the body and driven by an external circuit. The secondary coil is implanted with the device and connected to a receiver circuit. The coupled coils can move relative to one another as shown in Figure . As they move, their link voltage gain changes. Hence, good tolerance to axial and angular misalignment and coil separation is desired. Furthermore, to obtain large stimulating output voltage for the stomach and colonic stimulation, link voltage gain should be maximized for the required inductive link. Therefore, several factors should be taken into account when designing such an inductive link system. These factors include: (1) size of the transmitting and receiving coils, (2) link efficiency, (3) link voltage gain, (4) misalignment and separation tolerance, (5) communication bandwidth, and (6) overall size and complexity of the both transmitter and receiver.

According to Zierhofer and Hochkai [30], and Galbraith et al. [15], there are several advantages of developing a highly coupled inductive link which are applicable when designing a multi-channel gastrointestinal stimulation system.

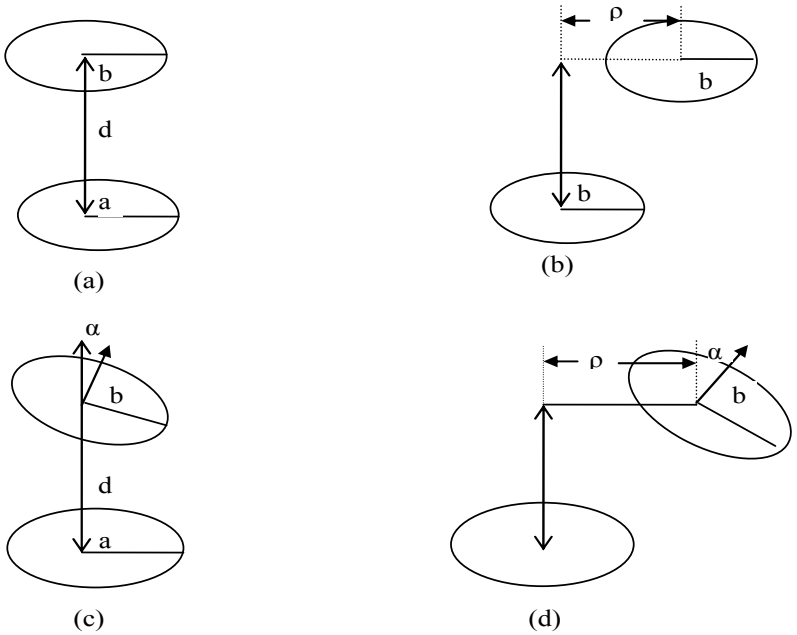

Figure 2: Coil alignments.
(a) Ideal alignment. (b) Lateral misalignment.
(c) Angular misalignment. (d) General misalignment.

1. The overall voltage gain is insensitive to variations of the relative position of the coupling coils.
2. The high coupling coefficient between the transmitter and the receiver reduces the current in the primary coil. This reduces the power dissipation in the primary side due to I^2R-losses. Thus the overall power transmission efficiency is enhanced.
3. The high coupling coefficient between the transmitter and the receiver reduces the magnitude of the required electromagnetic field, which in turn diminishes tissue heating.

2.3 Modeling the Highly Coupled Inductive Link

Galbraith et al (1987) [15] introduced four different combinations of highly coupled stagger-tuned inductive link. They were: (1) voltage in - voltage out, (2) voltage in - current out, (3) current in - current out, and (4) current in - voltage out. The "voltage in - voltage out" link is an approach which can control the output gain. This approach is based on coupling, not geometry. It not only corrects for lateral displacement, but also handles coil separation. The frequency response of such a link for various coupling coefficients k, in a frequency range of 0.5 - 3 MHz, is illustrated on Error! Reference source not found.. At a frequency of approximately 1.60 MHz, the variation in the gain is minimized, eventhough the coupling coefficient between the transmitter and the receiver varies from 0.26 to 0.54.

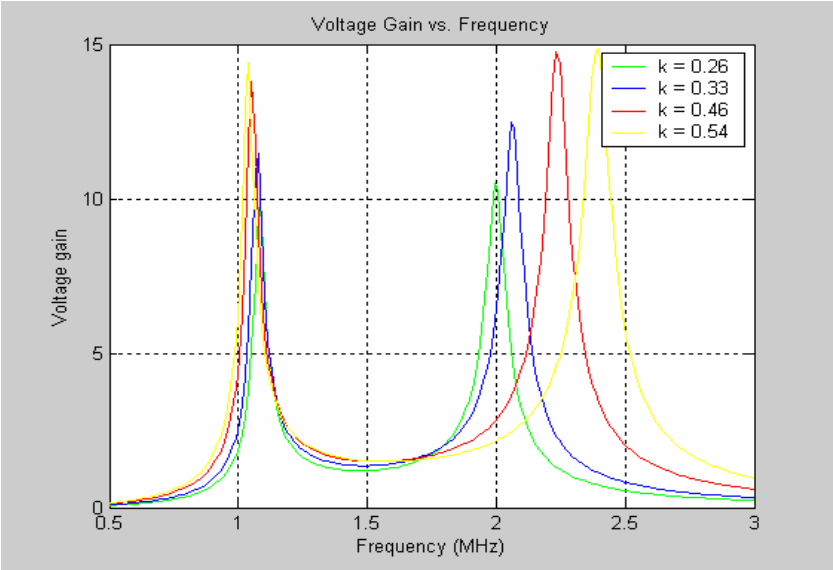

Figure 3: Voltage Gain of Stagger Tuned Inductive Link

In gastrointestinal electrical stimulation the properties of the stimulated tissue are dynamically different, and therefore the current consumption and loading of the inductive link would vary widely. This means that the gain of a transcutaneous inductive link should be stable over a wide range of coupling and loading impedances. A highly coupled link of the type "voltage in - voltage out" is to be preferred, because it can control the overall gain. The design procedure for such a link will be described in Section 2.5. A model of the highly coupled inductive link is depicted on Figure . On the primary side, the transmitter coil is tuned into a serial resonance with a capacitor Ct, so that appreciable coil current can be achieved from a sinusoidal voltage source. The receiver coil is tuned into a parallel resonance with a shunt capacitor Cr in order to obtain a high voltage output.

The expressions used to calculate the magnitudes of the unregulated DC load voltage and the DC power delivered to the load for the circuit model of Figure are described in [20].

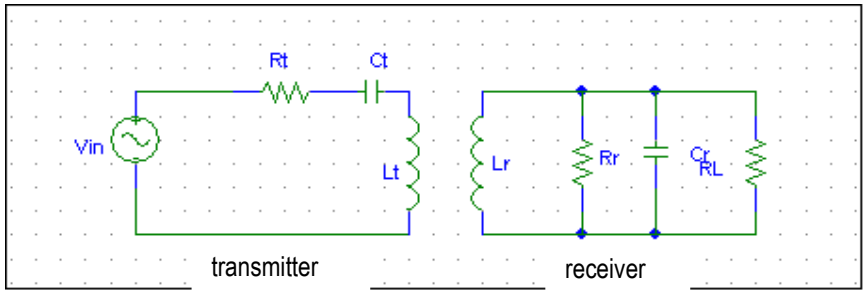

Figure 4: Simplified "Voltage in: Voltage out" circuit model of the stagger-tuned link

The impedance of the receiver is: $Z_{receiver} = Z_{real} + jZ_{imag}$. The equations used for this calculation are presented as follows:

$$P_{dc} = \frac{\left|V_{load}^2\right|}{R_{load}} \tag{2.3.1}$$

where P_{dc} is the DC power deliver to the load, R_{load} is impedance of the load in the receiver, and

$$\left|V_{load}\right| = \left|I_r\right| \sqrt{\left(\frac{2R_{load}}{4+\omega^2 C_r^2 R_{load}^2}\right)^2 + \left(\frac{\omega C_r R_{load}^2}{4+\omega^2 C_r^2 R_{load}^2}\right)^2} \tag{2.3.2}$$

where ω is the operating frequency, C_r is the shunt capacitor in the receiver, and

$$\left|I_r\right| = \frac{\left(\left|I_t\right|\omega R\right)}{\sqrt{\left(R_r + \frac{2R_{load}}{4+\omega^2 C_r^2 R_{load}^2}\right)^2 + \left(\omega L_r - \frac{\omega C_r + R_{load}^2}{\omega^2 C_r^2 R_{load}^2}\right)^2}} \tag{2.3.3}$$

where R_r is the equivalent series resistance of the receiver coil

$$\left|I_t\right| = \sqrt{\frac{(V_{in} Z_{real\_total})^2 + (V_{in} Z_{imag\_total})^2}{(Z_{real\_total}{}^2 + Z_{imga\_total}^2)}} \tag{2.3.4}$$

where

$$Z_{real\_total} = Z_{reflected\_real} + R_t \tag{2.3.5}$$

$$Z_{imag\_total} = Z_{reflected\_imag} + \left(\omega L_t - \frac{1}{\omega C_t}\right) \tag{2.3.6}$$

where R_t is the equivalent series resistance of the transmitter coil, C_t is the capacitor in the transmitter, and

$$Z_{reflected\_real} = \frac{\omega^2 M^2 Z_{real}}{Z_{real}^2 + Z_{imag}^2} \tag{2.3.7}$$

$$Z_{reflected\_imag} = \frac{-\omega^2 M^2 Z_{imag}}{Z_{real}^2 + Z_{imag}^2} \tag{2.3.8}$$

where M is the mutual inductance between the transmitter and receiver coils, and

$$Z_{real} = R_r - \frac{R_{load}/2}{1+\omega^2 C_r^2 (R_{load}/2)^2} \tag{2.3.9}$$

$$Z_{imag} = \omega L_r - \frac{\omega C_r (R_{load}/2)^2}{1+\omega^2 C_r^2 (R_{load}/2)^2} \tag{2.3.10}$$

In the above circuit model, the transmitter is usually powered by batteries utilizing a power amplifier. In order to power the transmitter and to avoid frequent battery replacements, it is required to be relatively efficient in converting DC to AC (RF) power. Class E power amplifier boasts a theoretical DC to AC conversion efficiency up to 95%, and is the most widely used transmitter topology used in transcutaneous power transformers. Therefore, Class E topology is routinely employed for powering the transmitter.

2.4 Class E Power Amplifier

Converters represent the primary portion of a power system. There are many types of converters such as (1) dc to ac, (2) ac to dc, (3) dc to dc, and (4) ac to ac.

The Class E power amplifier is an inverter which converts dc to ac voltage. It consists of a choke inductor L_{choke}, a power MOSFET utilized as a switch, a parallel capacitor C_p, and an *LC* resonant circuit (Figure 2.4). The switch turns on and off by a driver at a designated operating frequency f_o, and the LC resonant circuit oscillates at a frequency f_t. If f_o is equal to the resonant frequency f_t, the efficiency of Class E inverter is maximal. The choke inductor should have a high enough inductance to assure the ac ripple on the dc supply, I_{cc} (shown in Figure 5: Class E power amplifier) can be neglected [17]. In this case, the current through the choke inductor can be regarded as a steady current. When the switch is on, C_t and L_t function as a resonant circuit due to C_p being short-circuited by the switch, where f_t equals to $\frac{1}{\left(2\pi\sqrt{(L_t C_t)}\right)}$. When the switch turns off, C_p, C_t, and L_t form a resonant circuit, where f_t equals to $\frac{1}{\left[2\pi\sqrt{L_t C_t \frac{L_t C_t C_r}{(C_t + C_r)}}\right]}$. The advantages of Class E amplifier are zero power loss during the switching and high efficiency (about 95%) during the dc-to-ac power conversion. The capacitance C_t and the inductance L_t can be utilized to adjust the resonant frequency f_o. There are two important components, C_p and L_{choke}, which need to be determined. The capacitance C_p can be calculated by:

$$C_p = \frac{1}{(2\pi \times f_o \times R_t \times 5.477)} \tag{2.4.1}$$

where R_t is the resistance in the transmitter coil.

The choke inductor, L_{choke}, shown in Figure 5: Class E power amplifier is usually 3 – 10 times greater than the inductance of the transmitter coil [18].

Finally, the magnitude of the AC source of the transmitter, V_{in} (shown in Figure) is a function of DC supply powering the class E topology, and is calculated according to Eq. (2.4.2) [18, 19]

$$V_{in} = \frac{2V_{dc}}{\sqrt{1+\left(\frac{\pi^2}{4}\right)}} \tag{2.4.2}$$

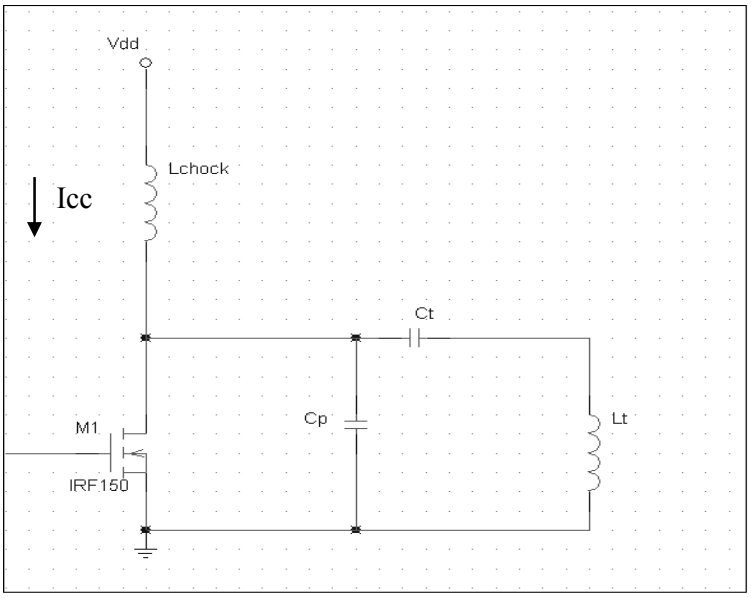

Figure 5: Class E power amplifier

2.5 Design of the Highly Coupled Inductive Link

2.5.1 Design Requirements

The voltage to be delivered to the implanted device would be in the range of 10 to 20 V DC for implanted stimulator current drawing between 0 and 50 mA [22]. The minimum and maximum equivalent loads are 200 Ω and 100 kΩ respectively [20]. The design requirements are presented in Table 1.

Design Requirement	Value
Minimum load voltage, V_{load}	10 V
Maximum load current, I_{load}	50 mA
Minimum value of load, $R_{loadmin}$	200 Ω
Maximum value of load, $R_{loadmax}$	100 kΩ
Power delivered to R_{load}	500 mW

Table 1: Highly coupled inductive link design requirement

2.5.2 Design Procedure

The design procedure of a stagger-tuned inductive link is outlined in [15] and is briefly described below.

Error! Reference source not found. shows that the minimum variation of gain of the inductive link occurs at 1.6 MHz. In the following procedure, it is assumed that the inductive link operates at an operating frequency of f_o = *1.6* MHz and the DC supply of the link is 9V.

2.5.2.1 Spiral Coil Design

In this project, the transmitter and receiver coils are both spiral coils and approximately of the same size. The methods used in calculating the self-inductance of such coils and the mutual inductance between the two coils have been previously reported [23, 13]. The calculation of the self-inductance of the spiral coils is based on the assumption that the spiral coils can be modeled as coaxial circular loops of wire.

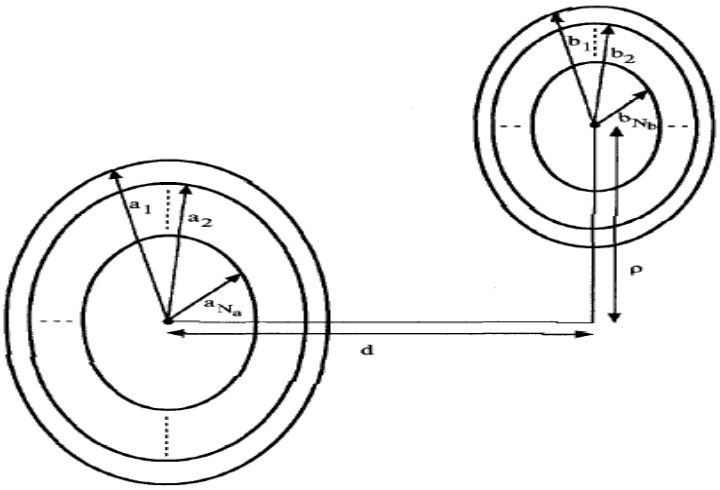

Figure 6: Geometric arrangement and notation for transmitter and receiver coils composed of circular concentric loops.

I. Calculation of the self-inductance of a spiral coil

The self-inductance of a single loop of wire can be calculated by:

$$L(a,w) = \mu_0 a\left(\ln\left(\frac{8a}{w}\right) - 2\right) \tag{2.5.1}$$

where a is the radius of the single loop, w is the radius of the wire, and μ_0 is the magnetic permeability of the free space.

The mutual inductance of two spiral coils whose axes are parallel can be presented by:

$$M(a,b,\rho,d) = \mu o\sqrt{ab}\left[\left(\frac{2}{k} - k\right)K(k) - \frac{2}{k}E(k)\right] \tag{2.5.2}$$

where

$$k \equiv \left(\frac{4ab}{(a+b)^2 + d^2}\right)^{\frac{1}{2}}$$

and where a and b are the radii of the two loops, d is the distance between the two loops, ρ is the axial misalignment, and K and E are the complete elliptic integrals of the first and second kind, respectively.

The self-inductance of such a coil is approximately equal to the summation of self-inductances of single loops, and with wire-radius w, the overall self-inductance is represented by:

$$L_a = \sum_{i=1}^{N_a} L(a_i, w) + \sum_{i=1}^{N_z}\sum_{j=1}^{N_a} M(a_i, a_j, \rho = 0, d = 0)(1 - \delta_{i,j}) \tag{2.5.3}$$

where $\delta_{i,j} = 1$ for $i = j$, and $\delta_{i,j} = 0$ otherwise.

II. Calculation of mutual inductance between two spiral coils

The mutual inductance between primary and secondary coils can be calculated by:

$$M_{ab} = \sum_{i=1}^{N_z} \sum_{j=1}^{N_a} M(a_i, b_j, \rho, d) \tag{2.5.4}$$

However, Eq. (2.5.4) is valid for the case with axial misalignment only. To calculate the exact mutual inductance between two coils with simultaneous axial and angular misalignments, an approximation s provided in [29]:

$$M(a,b,\rho,d,\alpha) = \frac{M(a,b,\rho,d)}{\sqrt{\cos\alpha}} \tag{2.5.5}$$

where α is the angular misalignment. Once the calculation method of self-inductance of a spiral coil and mutual inductance of two spiral coils is introduced, the parameters of transmitter and receiver coil orientations need to be determined. The constraints of the design are listed in Table 2.

Coil Separation	0.5 cm - 2.0 cm
Axial Misalignment	0 cm - ±1.0 cm
Angular Misalignment	0º - 20º
Diameter of transmitter and receiver coil	5 cm

Table 2: Highly coupled inductive link coupling constraints

Matlab code was developed for calculating the self-inductances and the mutual inductance of the transmitter (L_t) and the receiver (L_r) coils, based on the outlined constraints. The maximum and minimum coupling coefficients, k_{max} and k_{min}, are then calculated according to Eq. (2.5.6) and (2.5.7), respectively.

$$k_{\max} = \frac{M_{\max}}{\sqrt{L_t L_r}} \tag{2.5.6}$$

$$k_{\min} = \frac{M_{\min}}{\sqrt{L_t L_r}} \tag{2.5.7}$$

Furthermore, in order to determine the optimal number of turns, the Matlab Design Tool was used to vary the number of turns in the transmitter and receiver coils, and to compare the performance of the resulting links. In general, increasing the number of turns in the two coils reduced the variation in the load voltage, and enhanced the overall efficiency of the link. For this design, 10-turn spiral coils were chosen for the transmitter (n_t) and the receiver (n_r) coils. When the space between concentric turns of the coils is approximately 1.18 mm, the geometry of these coils results in a self-inductance L_t, L_r = 4.07 μH, with coupling coefficients k_{min} = 0.26 and k_{max} = 0.82.

2.5.2.2 Choosing the Operating Frequency fo

In order to minimize the amount of magnetic field absorbed by the abdominal tissue, the frequency should be chosen to be as low as possible, since the absorption increases exponentially with frequency [25]. However, the power transfer capability of the inductive link improves with increasing operating frequency. In addition, **Error! Reference source not found.** shows that at a frequency of approximately 1.60 MHz, the variation in the gain is minimized. Therefore, the frequency of f_o = 1.6 MHz was chosen as an operating frequency of the link.

2.5.2.3 Choosing the Resonant Frequency of the Receiver, fr

The resonant frequency of the receiver was chosen such that $f_r / f_o > 1$. The trade off is that as f_r / f_o increases, the overall voltage output gain increases. In other words, if the overall gain is too small, the ratio of f_r / f_o should be

moved away from unity. However, if the ratio of f_r / f_o increases, the overall gain variation also increases. To determine the optimal ratio of f_r / f_o, Matlab Design Tool was used to vary f_r / f_o and to compare the performance of the resulting links. Figure 7 shows different performances of the links with different ratios of f_r / f_o. After examining the magnitude and the variation of the load voltage for a set of values of f_r / f_o, it became apparent that for f_r / f_o = 1.2, the load voltage variation was minimized. This means the resonant frequency of the receiver was f_r = 1.92 MHz. The value of the shunt capacitor C_r can be calculated as follows:

$$c_r = \frac{1}{\omega^2 L_r} \tag{2.5.8}$$

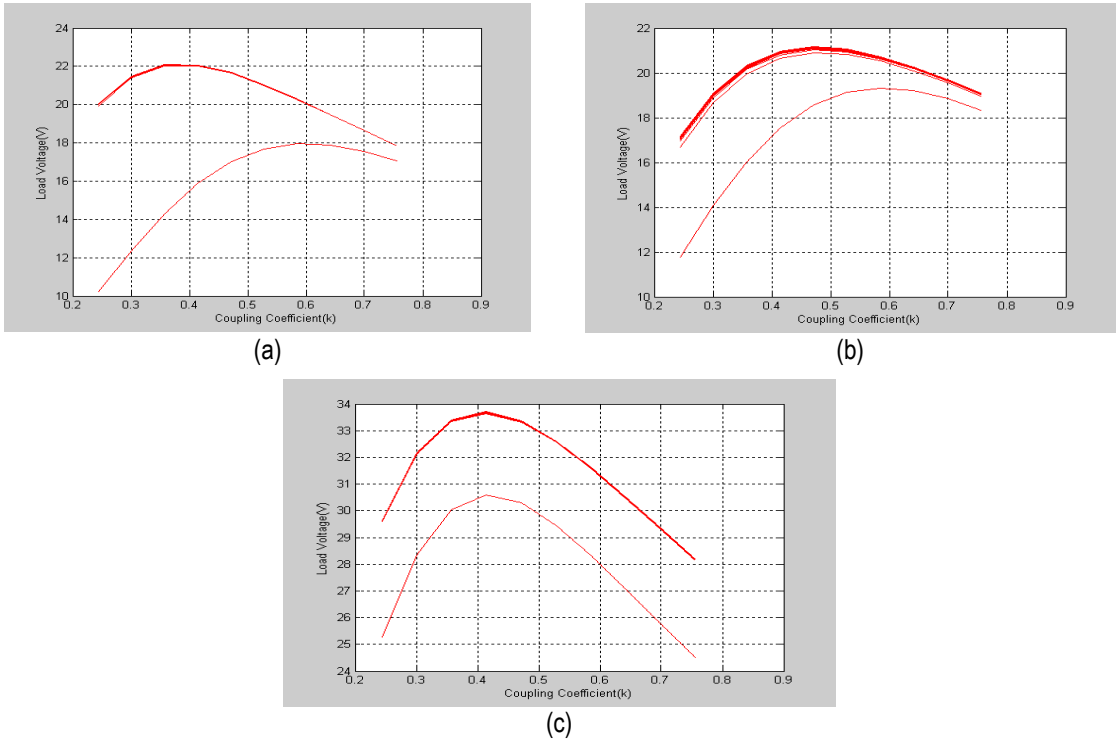

Figure 7: Load voltage over entire design space. (a) fr / fo = 1.1. (b) fr / fo = 1.2. (c) fr / fo = 1.4.

2.5.2.4 Choosing Resonant Frequency of Transmitter, ft

Next, the resonant frequency of transmitter, f_t, is calculated by Eq. (2.5.9) [11].

$$\omega_t = \sqrt{\frac{\left(\omega^2\right)\left(1 - H + \frac{1}{Q_t^2}\right)}{1 + \sqrt{H - \frac{1}{Q_T^2}}}} \tag{2.5.9}$$

Where

$$H = \frac{k_{opt}^4 \left[\left(\frac{\omega^2}{\omega_r^2}\right)^2 + \frac{1}{Q_r^2}\right]}{\left(1 - \frac{\omega^2}{\omega_r^2}\right) + \frac{1}{Q_r^2}} \tag{2.5.10}$$

and

$$k_{opt} = \sqrt{k_{\min} k_{\max}} \tag{2.5.11}$$

and

$$Q_t = \frac{\omega L_t}{R_t}, \quad Q_r = \frac{R_r}{\omega L_r} \tag{2.5.12}$$

With the determined tuning ratio, f_r / f_o, the receiver resonant frequency was determined with Eq. (2.5.13), and the transmitter resonant frequency was calculated as f_t = 1.12 MHz. The tuning capacitor of the transmitter is

$$c_t = \frac{1}{\omega^2 L_t} \tag{2.5.13}$$

Finally, Matlab Design Tool was used to determine the maximum and the minimum DC load voltages from the highly inductive link in order to specify the tolerance for the voltage regulation and other components for the rest of the transcutaneous energy transfer system. The plot of the maximum and the minimum load voltages for the inductive link is presented in Figure 8.

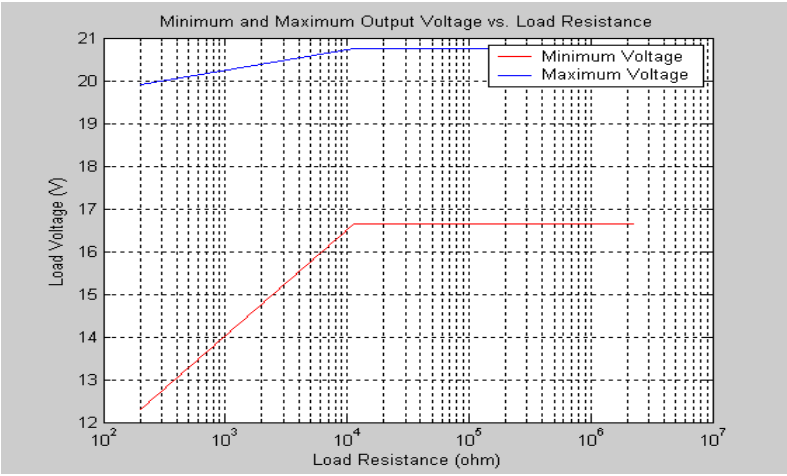

Figure 8: The maximum and minimum load voltage for the highly coupled inductive link.

3. Results

3.1 Spiral Coil Characterization

In order to reduce the power losses in the transmission load, Litz wire was used to make the spiral coils. Both the transmitter and the receiver coils were constructed using 270/46, 22 Gauge equivalent Litz wire (New England Electric Wire Corp., Lisbon, NH, USA). The number of turns in both coils was 10, and space between concentric turns of the coils was approximately 1.18 mm. There are two methods employed to validate the coil models, as described in Section 2.5.2.1. The first method is to use an LCR meter to extract the self-inductance and the equivalent series resistance (ESR) values from the coils. The values extracted from RLC meter for frequencies of 120 Hz, 1 KHz, and 10 KHz are presented in Tables 3, 4, and 5 respectively.

	Measured Self-inductance (μH)	Calculated Self-inductance (μH)	Percent Difference (%}	ESR (mΩ)
Transmitter coil	4.0	4.07	1.72	170
Receiver coil	4.05	4.07	0.49	170

Table 3: Self-inductance and ESR values extracted from RLC meter in 120 Hz

	Measured Self-inductance (μH)	Calculated Self-inductance (μH)	Percent Difference (%}	ESR (mΩ)
Transmitter coil	3.58	4.07	12.01	168
Receiver coil	3.77	4.07	7.37	168

Table 4: Self-inductance and ESR values extracted from RLC meter in 1 kHz

	Measured Self-inductance (μH)	Calculated Self-inductance (μH)	Percent Difference (%}	ESR (mΩ)
Transmitter coil	3.53	4.07	13.26	168
Receiver coil	3.71	4.07	8.85	168

Table 5: Self-inductance and ESR values extracted from RLC meter in 10 kHz

Measured values of self-inductance from the RLC meter at a low frequency (120 Hz in this case) agreed with the calculated values, while the percent difference between measured and calculated values increased with the increment of the operating frequency. This means that the self-inductance value of a spiral coil changes when the operating frequency changes. Alternatively, a testing circuit, depicted in Figure , was implemented to extract these same values. In the circuit, *R* was 10 Ohm and *C* was 1.78 nF. An *HP 33120A* function generator was used to drive the circuit. An *Agilent 54621D* oscilloscope measured the output voltage of the coils V_{out}. If the resistance of the circuit was small, the resonant frequency occurred at $\omega L = \frac{1}{\omega C}$. Also, the resonant frequency occurred when the impedance reaches maximum. The frequencies used for characterizing the circuit varied from 100 Hz to 3 MHz. Matlab Design Tool was used to plot the output voltages of the coil at various frequencies (Figure).

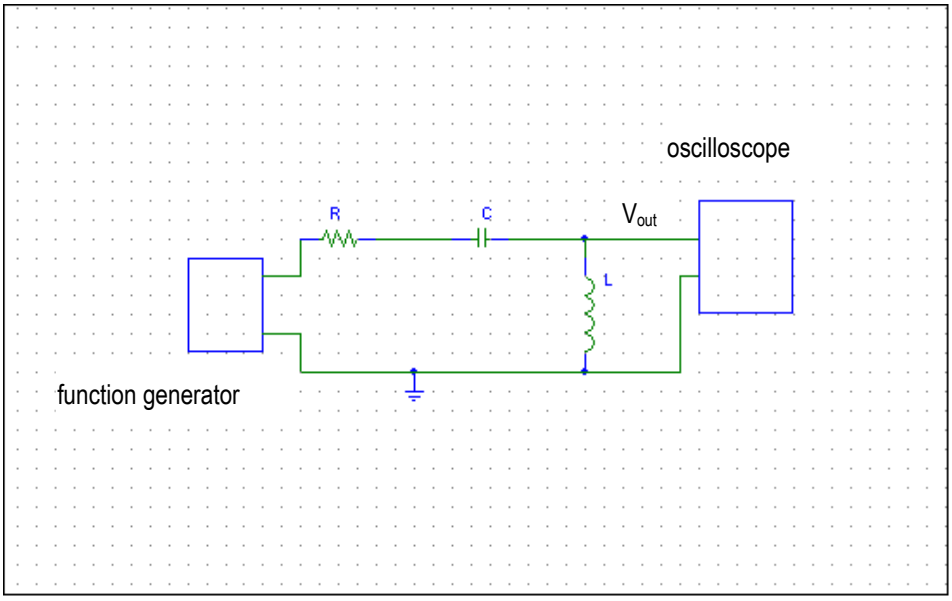

Figure 9: Serial resonant circuit for calculating the self-inductance of each coil

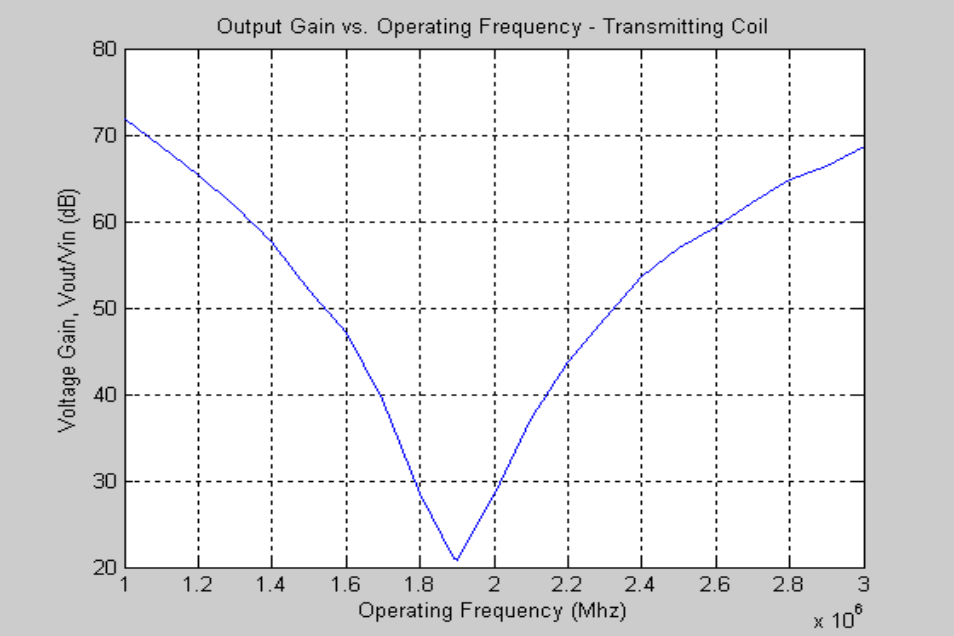

(a)

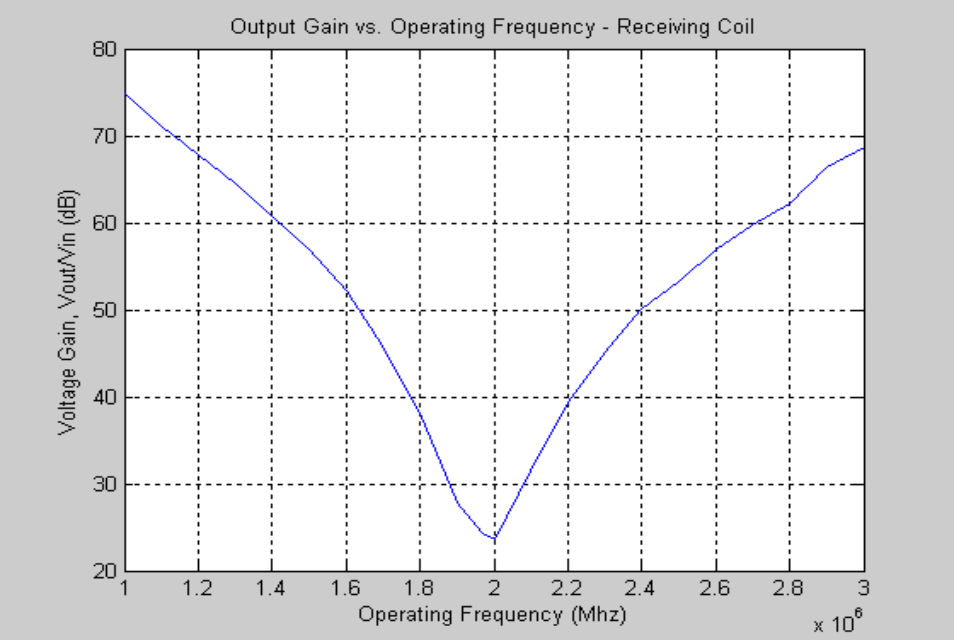

(b)

Figure 10: Frequency response of spiral coils. (a) transmitter coil; and (b) receiver coils.

Observing Figure , the resonant frequencies of the transmitter and the receiver coils were 1.9 MHz and 2.0 MHz, respectively. According to $L = \frac{1}{(2\pi f)^2 C}$, the self-inductance of the transmitter and the receiver coils can be calculated. The values of the self-inductance of the coils are shown in Table 6.

	Measured Self-inductance from resonant circuit (μH)	Calculated Self-inductance (μH)	Percent Difference (%)
Transmitter coil	3.52	4.07	13.5
Receiver coil	3.50	4.07	14.0

Table 6: Self-inductance values extracted from parallel resonant circuit

Comparison between the data from Tables 3, 4, and 5 shows that there is a gap greater than 10% between the measured and calculated values when frequency is higher than 1 kHz. The values in Table 6 were extracted from the frequency response of the resonant circuit. The circuit was built on a breadboard. The breadboard might affect the performance of the circuit. As a result, the difference between measured and calculated values in the above tables is reasonable, since the value of calculated inductance is frequency independent and the measured values of the self-inductance decrease with increasing the operating frequency. To obtain a more accurate result at the operating frequency of 1.6 MHz, a network analyzer is recommended.

3.2 Implementing the Highly Coupled Inductive Link

The implementation of the highly coupled inductive link is based on the coils characterized in the previous section. First, the implementation of the transmitter begins with the calculation of the component values of class E power amplifier according to the methodology described in Section 2.4. The values of the choke inductor, the parallel capacitor, and the series capacitor are listed in Table 7 below.

Component name	Value
Chock inductor, L_{chock}	33 μH
Parallel capacitor, C_p	12 nF
Series capacitor, C_t	3.3 nF

Table 7: Calculated values of the components in the transmitter

Second, the shunt capacitor and the filter capacitor in the receiver need to be determined. The value of the filter capacitor C_f can be calculated according to the voltage rise time required by the stimulator unit described in [21]. The values of both components, C_r and $C_{f,}$ are presented in Table 8.

Component name	Value
Filter capacitor, C_f	15 nF
Shunt capacitor, C_t	1.2 nF

Table 8: Calculated values of component in the receiver

3.3 Highly Coupled Inductive Link Testing

3.3.1 DC Output Voltage with Various Load Resistance

The measurement of the DC output voltage with various load resistances was based on a coil separation of 1.8 cm with an axial misalignment of 0° and an angular misalignment of 0°. The values of the resistive load varied from 100 Ω to 3.3 kΩ. The measured and calculated results are present on Figure 8.

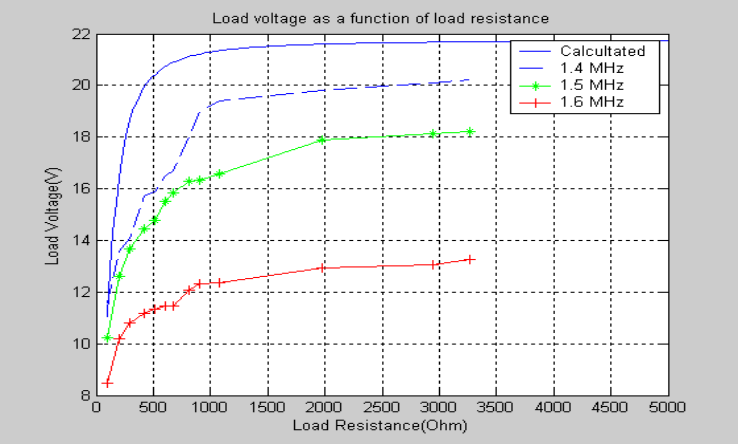

Figure 11: Measured and calculated values of the highly transcutaneous inductive link with various load resistances.

Figure 1 depicts the difference between the measured maximum and minimum load voltages, which is minimized when the operating frequency is 1.6 MHz. However, the difference between the calculated (ideal case) and measured load voltages is maximized at the same frequency. It is observed that the maximum variation between the measured maximum and minimum load voltages occurs at 1.4 MHz. To optimize the transcutaneous inductive link, 1.5 MHz is chosen as the operating frequency for the link, instead of 1.6 MHz, which was discussed in Section 2.5.

3.3.2 Coil Tolerance

All measured and calculated results presented in this section were based on a DC power supply of 9 V in the transmitter, with a 1 kΩ load in the receiver. The operating frequency of the transcutaneous inductive link was 1.5 MHz. The voltage drop across two Schottky diodes (about 0.8 V) of the full-wave bridge in the receiver was also subtracted from the model.

I. Separation Tolerance

The transmitter and the receiver coils in the highly inductive link operate at separation range of 5 – 25mm. Both calculated and measured values are plotted in Figure 12.

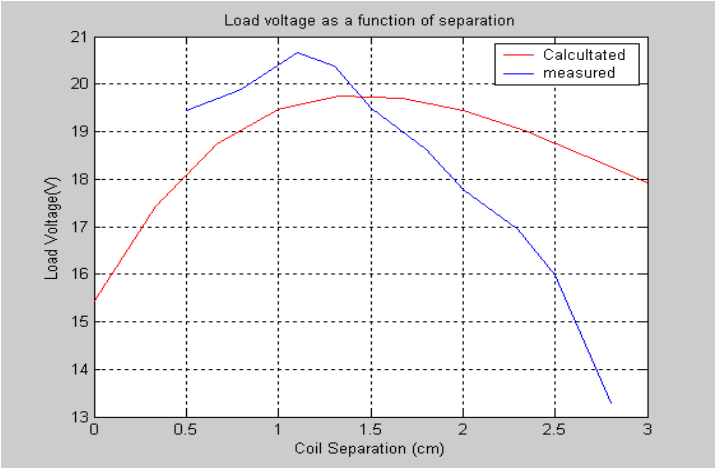

Figure 12: Comparison between calculated and measured coil separation tolerances in the highly coupled trancutaneous inductive link

The maximum measured and calculated values were observed when the coil separation was about 1.5 cm. The variation of measured and modeled values was greater than 10%. However, the minimum measured value was 16 V which was within the range of desired DC load voltage (10 V – 20 V).

Angular tolerance

The measurement of the angular tolerance was based on the coil separation of the transmitter and the receiver coils of 1.5 cm. The range of the angular misalignment was between 0° and 20°. Measured and calculated results are depicted on Figure 13.

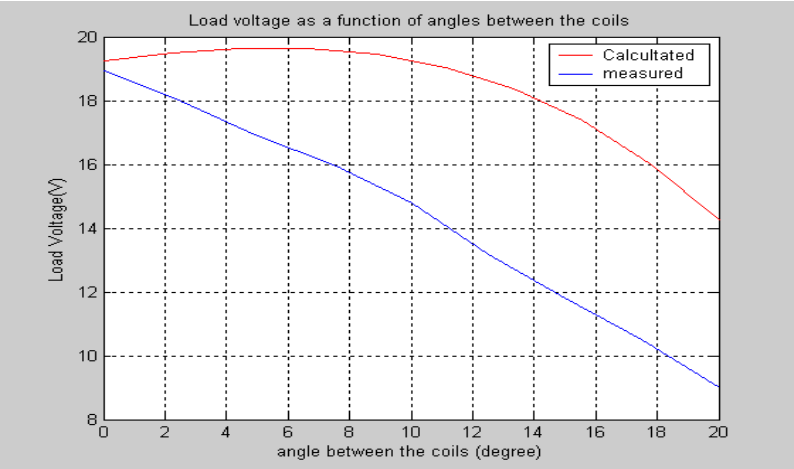

Figure 13: Comparison of calculated and measured angular misalignment tolerance in the highly coupled trancutaneous inductive link.

The slope of the measured values is much higher than the slope of the calculated values. However, the measured value at 18° is still within the desired DC load voltage (10 V – 20 V).

Axial misalignment tolerance

The measurement of the axial misalignment tolerance was based on a load resistance of 200Ω and 1.5 cm separation between the transmitter coil and the receiver coil. The range of the axial misalignment was between 0 and 1cm. The measured and calculated results are plotted on Figure 3.5, which shows that the difference between the measured and the modeled values of axial misalignment is within 12%.

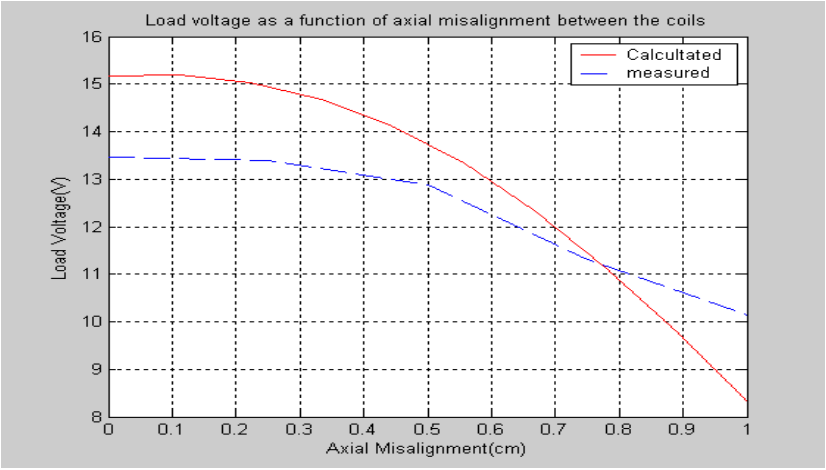

Figure 14: Comparison of the calculated and measured axial misalignment tolerance in the highly coupled trancutaneous inductive link

Power Transfer Efficiency

One may be interested in the overall power transfer efficiency η of a highly coupled transcutaneous inductive link. Under a typical coupling condition, with a coil separation of 15 mm, and 5 mm of axial misalignment, the overall DC power from the transmitter was delivered to a DC load ranging from 100Ω to 3200Ω,as presented in Figure 14. The overall energy transfer efficiency of the transcutaneous energy transformer is presented in Figure 15.

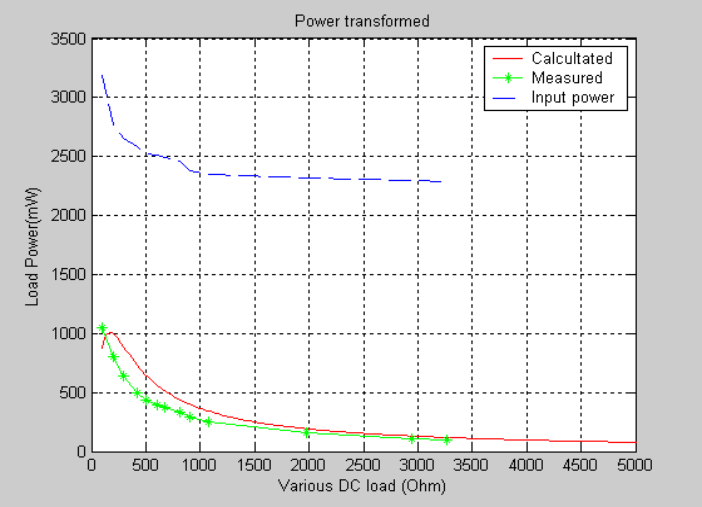

Figure 15: Input power from the transmitter, calculated and measured power to the implanted load

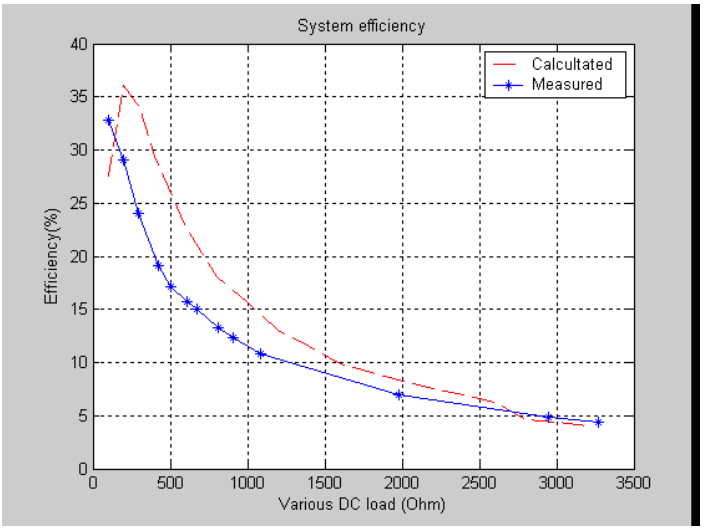

Figure 16: Overall power transfer efficiency of the highly transcutaneous inductive link.

Figure 15 reveals that the overall energy transfer efficiency is maximized at 33% when the DC load, R_{load}, is 100Ω. When R_{load} is 200Ω, the efficiency reaches 28%.

Conclusion

In this report a comprehensive design and testing of a transcutaneous energy transfer system for an implanted system is provided, specifically targeted for gastrointestinal stimulation. The robust modeling of the transcutaneous transformer has been validated through the design, implementation, and testing stages. The measured results for the transformer are in a good agreement with the predicted values.

Bibliography

[1] J.E. Everhart (Ed). Digestive Diseases in the United States: Epidemiology and Impact. National Institutes of Health Publication No. 94-1447, 1994

[2] A. M. Bilgutay, R. Wingrove, W. O. Grifen, R. C. Bonnabeau, C.W. Lillehei. Gastro-intestinal pacing: a new concept in the treatment of ileus. Annals of Surgery, 158(3), 139-144, 1963.

[3] J.D. Huizinga. Electrophysiology of human colon motility in health and disease. Clinics in Gastroenterology, 15(4), 879-901. 1986.

[4] S. Grundfest-Bronialowski, A. Moritz, E. Olsen, J. Kasick, L. Ilyes, G. Jacobs, and U. Nose. Electrical control of intestinal reservoirs in a chronic dog model. ASAIO Transactions, 34:664-668, 1988.

[5] E.L. Chaffee and R.E. Light. A method for remote control of eclectrical stimulation of the nervous system. Yale J. Biol. Med., 7, 1934.

[6] T. Cameron, G.E. Leob, R.A. Peck, J.H. Schulman, P.Strojnik, and P.R. Troyk. Micro modular implants to provide electrical stimulation of paralyzed muscles and limbs. IEEE Trans. Biomed. Eng., 44(9):781-790, September 1987.

[7] K. Bruninga, L, Reidy, A. K eshaveersian, et al. The effect of electrical stimulation on colonic transit following spinal cord injury in cats. Spinal cord. 36:847-53, 1998.

[8] S. Grundfest-Broniakowski, A. Moritz, L. Ilyes, et al. voluntary control of and ideal pouch by coordinated electrical stimulation, a pilot study in the dog. Dis Colon Rectum. 31:261-7, 1998

[9] S.F. Hughes, S.M. Scott, MA Pilot, et al. electrically stimulated smooth muscle neosphincter. Br J Surg. 82:1321-61, 996.

[10] M. P. Mintchev, C. P. Sanmiguel, M. Amaris, K. L. Bowes. Microprocessor controlled movement of solid gastric content using sequential neural electrical stimulation. Gastroenterology, 118, 258-263. 2000.

[11] M. P. Mintchev, C. P. Sanmiguel, S. G. Otto, K. L. Bowes. Microprocessor controlled movement of liquid gastric content using sequential neural electrical stimulation. Gut, 43, 607-611, 1998.

[12] M.P. Mintchev and K.L. Bowes. Computer model of gastric electrical stimulation. Ann. Biomed. Eng., 25:726-730, April 1997.

[13] W.H. Ko, S.P. Liang, and C.D.F. Fung. Design of radio-frequency powered coils for implant instruments. Med. & Biol. Eng. & Comput., 15:634-640, 1977.

[14] N. de N. Donaldson and T.A. Perkins. Analysis of resonant coupled coils in the design of radio frequency transcutaneous links. Med. & Biol. Eng. & Comput., 21:612-627, 1983.

[15] D.C. Galbraith, M. Soma, and R.L. White. A wide-band efficient inductive transdermal power and data linkwith coupling insensitive gain. IEEE Trans. Biomed. Eng., 34(4):265-275, April 1987.

[16] O. Soykan, Power sources for implantable medical devices, Device Technology & Application ELECTRONICS. 2002.

[17] M. K. Kazimierzuk, D. Czarkowski. Resonant power converters. Wiley-Interscience Publication, 1995, ISBN 0-471-04706-6.

[18] Nathan O. Sokal, Alan D. Sokal. Class E – A new class of high-efficiency tuned single-ended switching power amplifiers. IEEE Journal of solid-state circuits, vol. SC-10, No. 3, June 1975

[19] F.H. Raab. Idealized operation of the class E tuned power amplifier. IEEE Trans. Cir. Sys., CAS-24(12):725-735, December 1977.

[20] J.A. Doherty, G.A. Julien, M.P. Mintchev. Trancutaneous powering of implantable micro-stimulators for functional restoration of impaired gastrointestinal motility. In proceeding of the 25th Annual International Conference of the IEEE EMBS of the IEEE Engineering in Medicine and Biology Society, Cancun, Mexico, 2003, pages 1575-1578, 2003.

[21] J. Doherty. Implantable, transcutaneously powered neurostimulator system to restore gastrointestinal motility. M.Sc. Thesis, University of Calgary, Calgary, Alberta, Canada, 2005.

[22] D. Onen. Implantable, transcutaneously powered neurostimulator system to restore gastrointestinal motility. M.Sc. Thesis, University of Calgary, Calgary, Alberta, Canada, 2005.

[23] C. M. Zierhofer, E. S. Hochmair. Geometric approach for coupling enhancement of magnetivally coupled coils. IEEE Trans. Biom. Eng., 43(7):708-714, July, 1996.

[25] T. Akin. An integrated telemetric mulit-channel sieve electrode for nerve regerneration applications. Ph.D. dissertation, University of Michiagan, Ann, Arbor, MI, USA, 1994

Authors' Information

Joanna Liu C. Wu *– undergraduate Student, Department of Electrical and Computer Engineering, University of Calgary, Calgary, Alberta, Canada T2N1N4;e-mail: joannawu@enel.ucalgary.ca*

Major Fields of Scientific Research: Embedded Systems, Electronic Instrumentation

Martin P. Mintchev *– Professor, Department of Electrical and Computer Engineering, University of Calgary, Calgary, Alberta, Canada T2N1N4; Fellow, American Institute for Medical and Biological Engineering, Washington, DC, USA; e-mail: mintchev@ucalgary.ca*

Major Fields of Scientific Research: Biomedical Instrumentation, Navigation, Information Systems in Medicine